This article has been accepted for publication in a future issue of this journal, but has not been fully edited. Content may change prior to final publication. Citation information: DOI 10.1109/OJAP.2021.3078234, IEEE Open Journal of Antennas and Propagation

Bessel–Gauss Beam Launchers for Wireless Power Transfer

Srđan Paković, Siyi Zhou, David González-Ovejero, Santi Concetto Pavone, Anthony Grbic, and Mauro Ettorre

In this work, we study the use of Bessel–Gauss beam launchers for wireless power transfer (WPT) applications. The power transfer efficiency between two radiating apertures is investigated in the radiative near field. A spectral Green's function approach is used to derive the power efficiency under a simultaneous conjugate impedance match. The transverse electromagnetic (TEM) mode of a coaxial cable, as well as Bessel beam (BB) and Bessel–Gauss beam (BGB) field distributions, are considered as aperture distributions. Numerical results demonstrate that a BGB field distribution is the optimal choice for WPT due to its limited spectrum and reduced diffraction of the radiated beam. We synthesized a Bessel–Gauss launcher that exhibits power efficiency exceeding 50% for distances larger than 30λ. These results show that non-diffracting beams can pave the way toward efficient near-field WPT systems with extended operating ranges.

***Index Terms*—Bessel–Gauss beams, non-diffracting beams, wireless power transfer, Bessel beams, horn antennas**

I. Introduction

The concept of wireless power transmission was introduced by Tesla in the 1890s [1]. The basic idea involves transferring electrical power without a wired connection between the transmitter (Tx) and the receiver (Rx). In recent years, the topic of WPT has been revived due to the surge in portable electronic devices and limited battery capacity. The possibility to recharge wirelessly will truly 'unplug' such devices. The coupling mechanism used in current WPT systems is based on an electromagnetic interaction between the Tx and Rx in their reactive near-field or far-field regions.

Reactive near-field WPT systems are generally based on an inductive or capacitive coupling mechanism with operating frequencies in kHz and MHz range. The operating distance of such systems is on the order of the lateral size of the Tx and therefore much smaller than the free space wavelength [2], [3]. Far-field WPT systems use a radiated wave to transfer energy, and thus their operating distances can be much larger. On the other hand, such an approach suffers from low efficiency [4], [5].

Today, near-field WPT systems are employed to recharge electronic accessories [6], [7]. A charging pad is generally used and the operating range is limited to a few centimeters.

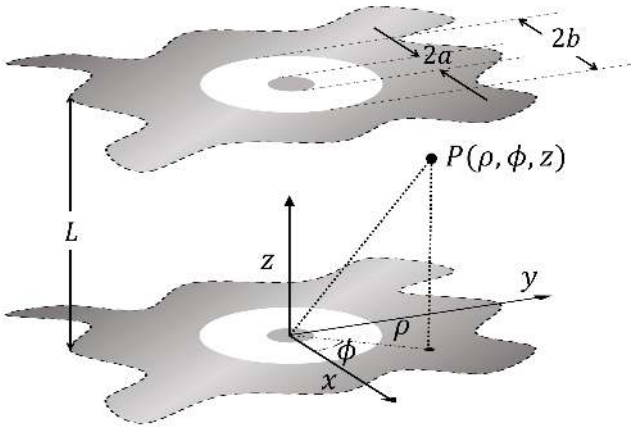

Fig. 1. Graphical representation of the considered WPT configuration. The radiating apertures are located in infinite metallic ground planes that form a PPW environment between the two apertures.

In order to extend the operating distance, the power transfer efficiency over distance must be improved [6].

In [8], power transfer efficiency was studied in the Fresnel zone between two radiating apertures under a paraxial approximation. The transfer efficiency was treated as an eigenvalue problem to derive the optimal aperture field that maximizes power transfer efficiency. An optimal aperture was found to be a spheroidal function for the case of linear-polarized rectangular apertures. The proposed solution is valid in the Fresnel zone of the radiating apertures, but does not consider the mutual interaction between the two apertures. In [9], the possibility of employing Bessel beams [10] for power transfer was investigated and efficient power efficiency was demonstrated. In [11], [12], a Green's function approach was adopted to study wireless power transfer between small radiators.

In more recent work [13], the power transfer efficiency of

This work was supported in part by the Ministry of Higher Education and Research, Brittany and Rennes Métropole, through the Contrat de plan État-Région (CPER) and in part by the Université de Rennes 1.

S. Paković and S. Zhou contributed equally to this work as first authors.

S. Paković, S. Zhou, D. González-Ovejero, and M. Ettorre are with Univ Rennes, CNRS, IETR (Institut d'Électronique et des Technologies du numéRique), UMR 6164, F-35000 Rennes, France (e-mail: srdan.pakovic@univ-rennes1.fr, david.gonzalez-ovejero@univ-rennes1.fr, mauro.ettorre@univ-rennes1.fr)

S. C. Pavone is with the Department of Electrical, Electronics and Computer Engineering (DIEEI), University of Catania, Viale Andrea Doria 6, 95125 Catania, Italy (e-mail: santi.pavone@unict.it)

A. Grbic is with the Radiation Laboratory, Department of Electrical Engineering and Computer Science, and the Center for Photonic and Multiscale Materials (C-PHOM), University of Michigan, Ann Arbor, MI 48109-2122 USA (e-mail: agrbic@umich.edu)

S. C. Pavone would like to thank the project PON-AIM "Attraction and International Mobility", granted by the Italian Ministry of Education and Scientific Research (MIUR).

This article has been accepted for publication in a future issue of this journal, but has not been fully edited. Content may change prior to final publication. Citation information: DOI 10.1109/OJAP.2021.3078234, IEEE Open Journal of Antennas and Propagation

a WPT link using cylindrical vector beams was studied using an approach similar to [8]. It was concluded that Bessel and Bessel–Gauss beams could be a good choice for WPT systems compared to Gaussian beams. The BGB is essentially a Bessel beam truncated by a Gaussian profile, which exhibits nearly diffraction-free properties up to a certain distance called the non-diffractive range (NDR) [14]–[17]. The main advantage of BGBs to BBs is that the radial modulation tapers the aperture fields, reducing the on-axis ripples caused by edge diffraction. In [17], the authors numerically obtained an expression for the NDR of BGBs and demonstrated that their NDR depends heavily on the width of the Gaussian window, i.e., apodization factor. More precisely, the NDR of BGBs is either less or equal to the NDR of BBs. Therefore, by tuning the apodization factor, we can reduce the edge diffraction without affecting the non-diffractive range. However, the radial modulation enforced by the Gaussian window may affect the self-healing property peculiar to Bessel beams, which is mostly associated to its outer rings [18]. In literature, several works compare the non-diffractive performance of Gaussian beams, BBs, and BGBs [19]–[21] with similar findings.

In this paper, we investigate the use of Bessel–Gauss beam launchers for WPT. We have extended the work in [9], [13] by evaluating the power transfer efficiency between two radiating apertures in their near-field zone considering their mutual interaction. We approximate the mutual interaction by assuming a parallel-plate waveguide (PPW) environment formed by the two infinite ground planes supporting the apertures. We use the spectral Green's function of the PPW to solve the electromagnetic problem of two coupled apertures. An equivalent circuit representation of the system based on an admittance matrix is then proposed. The power transfer efficiency is derived assuming a simultaneous conjugate impedance match. The results are validated by deriving the transmitted and received power using the Poynting vector of the radiated fields, as in [8]. We have presented and compared three types of aperture fields for WPT: the TEM mode of a coaxial cable, BB, and BGB aperture. We demonstrate that the BGB is the optimal choice for WPT due to its narrow spectrum and reduced diffraction of the radiated beam. Applying the procedure introduced in [22], we synthesized a BGB launcher. We have shown that the launcher is capable of transfering power wirelessly over several tens of wavelengths with high efficiency (60% over 30λ). We have also shown that the WPT efficiency exhibits large fluctuations for longer distances. Finally, we have introduced a frequency tuning technique to smooth out these fluctuations in efficiency.

II. Geometry of the Problem

The geometry of the problem considered is shown in Fig. 1. Two circular apertures of the same radius are placed onto parallel and infinite ground planes. The infinite ground planes form a PPW environment between the two apertures. The apertures correspond to the Tx and the Rx of the WPT system. The Tx aperture is perpendicular to the z-axis and centered at the origin of a cylindrical coordinate system. The Rx aperture is parallel to the Tx aperture and located at a distance $z = L$. Both apertures are azimuthally symmetric and axially aligned. In this paper, vectors will be denoted by bold characters, unit vectors by bold characters with a caret, and matrices by bold characters underlined by double bars. An $e^{j\omega t}$ time dependence is assumed, where ω is the angular frequency. In order to derive the power transfer efficiency, a spectral Green's function approach is employed. Specifically, the radiated and received fields are calculated once a tangential field distribution is imposed over the radiating apertures. Throughout this paper, three aperture distributions are considered, namely the field profile of the TEM mode of a coaxial cable, BB, and BGB distributions. It is worth noting that in the following, we will consider Transverse Magnetic (TM) modes without loss of generality. Indeed, Section V will validate the analysis with a launcher based on a Transverse Electric (TE) mode. Nevertheless, the non-diffractive range is determined solely by the radial spectral wavenumber and the aperture size, not the polarization, as demonstrated in Section VI of [22].

A. Spectrum of the aperture fields

The spectrum of the transverse equivalent magnetic current distribution of the TEM distribution can be expressed as

$$\widetilde{\boldsymbol{M}}(k_\rho) = j2\pi \frac{V_0 \left(J_0(k_\rho b) - J_0(k_\rho a)\right)}{\ln(b/a) k_\rho} \hat{\boldsymbol{\phi}} \tag{1}$$

where $\hat{\boldsymbol{\phi}}$ is the azimuthal unit vector; V_0 is the amplitude of the distribution, referred to as "voltage" [23] ; a is the outer radius of the coaxial cable and b is the radius of the inner conductor (please refer to Fig. 1); k_ρ is the radial spectral wavenumber and $J_n(\cdot)$ is the n-th order, first kind Bessel function.

The spectrum of truncated Bessel field distribution is given by [24]

$$\widetilde{\boldsymbol{M}}(k_\rho) = \frac{a}{k_1^2 - k_\rho^2} \left[k_\rho J_0(k_\rho a) J_1(k_1 a) - k_1 J_0(k_1 a) J_1(k_\rho a)\right] \hat{\boldsymbol{\phi}} \tag{2}$$

where a is the radius of the circular aperture (refer to Fig. 1), and $k_1 = x_{0n}/a$, where x_{0n} is the zero of the Bessel function (or its derivative) of the corresponding Bessel beam. [25], [26]. The non-diffractive range of BBs is given by

$$z_{\mathrm{ndr}}^{\mathrm{BB}} = a\sqrt{\left(\frac{k}{k_1}\right)^2 - 1}. \tag{3}$$

As for the spectrum of the Bessel–Gauss distribution, it is a finite Hankel transform which is typically hard to express analytically and computationally expensive to calculate. However, the Bessel–Gauss distribution tends to zero at infinity. If the apodization width $w_0 < a$, the spectrum of the Bessel–Gauss distribution can be approximated with the infinite Hankel transform, as

$$\widetilde{\boldsymbol{M}}(k_\rho) = \frac{w_0^2}{2} e^{-\frac{w_0^2(k_1^2 + k_\rho^2)}{4}} \cdot I_1\Big(\frac{w_0^2 k_1 k_\rho}{2}\Big) \hat{\boldsymbol{\phi}} \tag{4}$$

where $I_n(\cdot)$ is the modified Bessel function of the first kind of order n. The NDR of BGBs is given by [17]

$$z_{\mathrm{ndr}}^{\mathrm{BGB}} = \begin{cases} z_{\mathrm{ndr}}^{\mathrm{BB}} \tilde{w}_0 \sqrt{\ln 4}, & \tilde{w}_0 < \dfrac{1}{\sqrt{\ln 4}}, \\ z_{\mathrm{ndr}}^{\mathrm{BB}}, & \tilde{w}_0 \geq \dfrac{1}{\sqrt{\ln 4}}, \end{cases} \tag{5}$$

where $z_{\mathrm{ndr}}^{\mathrm{BB}}$ denotes the NDR of the corresponding untapered BB (see Eq. (3)), and $\tilde{w}_0 = w_0/a$. Hence, depending on the choice of w_0, the NDR of the BGB can be either less or equal compared to the NDR of the corresponding BB.

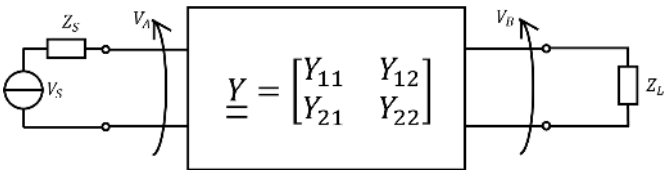

Fig. 2. Equivalent 2-port network representation of the two radiating apertures.

III. Power Transfer Efficiency

In this section, power transfer efficiency is derived using three different approaches based on a spectral Green's function formulation. We will refer to them as "equivalent network approach", "power flow approach", and "T-factor approach", respectively.

In the equivalent network approach, the two radiating apertures are modeled as a 2-port network. Knowledge of the fields radiated and received by the apertures is used to derive an admittance matrix representation of the 2-port network. The power transfer efficiency of the network is obtained through network analysis.

The power flow approach uses the fields radiated and received by the apertures to derive the ratio of the power accepted by the receiving aperture over the power radiated by the transmitting one.

The T-factor approach is based on the transmission coefficient proposed in [27] and employed in [8], [13]. Here, the transmission coefficient is a function of the total electromagnetic field generated by the two apertures.

A. Equivalent Network Approach

The 2-port network representation of the system is shown in Fig. 2. In particular, we are interested in the admittance matrix representation of the system [28],

$$\underline{\underline{Y}} = \begin{bmatrix} Y_{11} & Y_{12} \\ Y_{21} & Y_{22} \end{bmatrix}. \tag{6}$$

Assuming equal apertures and reciprocity, the admittance matrix simplifies to $Y_{11} = Y_{22}$ and $Y_{12} = Y_{21}$.

By following the steps outlined in [28], [29] the elements of the admittance matrix can be derived as

$$Y_{11(22)} = \frac{1}{V_{\mathrm{ref}}^2} \frac{1}{(2\pi)^2} \int_{-\infty}^{\infty} \left| \widetilde{M}_\phi \right|^2 G_{\phi\phi}^{\mathrm{HM}}(k_\rho, z=0) k_\rho dk_\rho, \tag{7}$$

$$Y_{12(21)} = \frac{1}{V_{\mathrm{ref}}^2} \frac{1}{(2\pi)^2} \int_{-\infty}^{\infty} \left| \widetilde{M}_\phi \right|^2 G_{\phi\phi}^{\mathrm{HM}}(k_\rho, z=L) k_\rho dk_\rho, \tag{8}$$

where V_{ref} is the reference voltage associated with the aperture field, as defined in [30]; $\widetilde{M}_\phi$ is the Hankel transform of the equivalent magnetic current distribution along ϕ; $G_{\phi\phi}^{\mathrm{HM}}(z)$ is the spectral Green's function of the PPW environment describing the ϕ-component of the magnetic field due to a ϕ-oriented magnetic current.

Under simultaneous conjugate impedance match, the power transfer efficiency η is maximized and is equal to [31]

$$\eta = \frac{\Re\{Z_{\mathrm{L}}\}}{\Re\{Z_{\mathrm{in}}\}} \left| \frac{Z_{21}}{Z_{22} + Z_{\mathrm{L}}} \right|^2 \tag{9}$$

with Z_{12} and Z_{21} being the elements of the impedance matrix representation ($\underline{\underline{\boldsymbol{Z}}} = \underline{\underline{\boldsymbol{Y}}}^{-1}$) of the 2-port network and both the source (Z_{S}) and the load (Z_{L}) impedances satisfying the condition of the simultaneous conjugate match.

B. Power Flow Approach

In the power flow approach, the power transfer efficiency is defined as the ratio of the power accepted by the receiving aperture to the power radiated by the transmitting one. The electromagnetic problem is solved to derive the electric and magnetic fields radiated and received by the two apertures with TEM, BB, and BGB aperture distributions.

The first step is to derive the total electromagnetic field between the two apertures. By total electromagnetic field, we refer to the field generated when one aperture is excited and the other is terminated with a load. To do so, the radiating apertures are replaced by equivalent magnetic currents over a ground plane. The spectral Green's function of the PPW is then used to derive the radiated fields. In particular, the total magnetic and electric spectral field distributions can be expressed as

$$\widetilde{\boldsymbol{H}}_{\mathrm{tot}}(k_\rho, z) = \left[V_{\mathrm{A}} \widetilde{M}_\phi G_{\phi\phi}^{\mathrm{HM}}(k_\rho, z) + V_{\mathrm{B}} \widetilde{M}_\phi G_{\phi\phi}^{\mathrm{HM}}(k_\rho, z-L) \right] \hat{\boldsymbol{\phi}}, \tag{10}$$

$$\widetilde{\boldsymbol{E}}_{\mathrm{tot}}(k_\rho, z) = \left[V_{\mathrm{A}} \widetilde{M}_\phi G_{\rho\phi}^{\mathrm{EM}}(k_\rho, z) + V_{\mathrm{B}} \widetilde{M}_\phi G_{\rho\phi}^{\mathrm{EM}}(k_\rho, z-L) \right] \hat{\boldsymbol{\rho}}, \tag{11}$$

where $\widetilde{\boldsymbol{H}}(\widetilde{\boldsymbol{E}})_{\mathrm{tot}}$ is the total magnetic (electric) spectral field distribution; V_{A} and V_{B} are the equivalent voltages of the transmitting and the receiving aperture and $\widetilde{M}_\phi$ [23] is the Hankel transform of the considered equivalent magnetic current as given in Section II; $G_{\rho\phi}^{\mathrm{EM}}$ is the spectral Green's function of the PPW describing the radial component of the magnetic field due to the ϕ-oriented magnetic current. In (10) and (11), the total electromagnetic field is expressed as the sum of two components. Each component represents the contribution of each aperture to the total field. Let us consider the total magnetic field as an example. In (10), the first component of the sum, $V_{\mathrm{A}} \widetilde{M}_\phi G_{\phi\phi}^{\mathrm{HM}}(k_\rho, z)$, corresponds to

This article has been accepted for publication in a future issue of this journal, but has not been fully edited. Content may change prior to final publication. Citation information: DOI 10.1109/OJAP.2021.3078234, IEEE Open Journal of Antennas and Propagation

the contribution of the transmitting aperture. On the contrary, the second term $V_{\rm B}\widetilde{M}_{\phi}G^{\rm HM}_{\phi\phi}(k_\rho, z-L)$ is the contribution of the receiving aperture. The equivalent voltages $V_{\rm A}$ and $V_{\rm B}$ are related by the admittance matrix $\underline{\underline{\boldsymbol{Y}}}$ mentioned in the previous subsection, as

$$\begin{bmatrix} I_{\rm S} \\ 0 \end{bmatrix} = \left[\underline{\underline{\boldsymbol{Y}}} + \begin{bmatrix} Y_{\rm S} & 0 \\ 0 & Y_{\rm L} \end{bmatrix}\right] \begin{bmatrix} V_{\rm A} \\ V_{\rm B} \end{bmatrix}. \tag{12}$$

In (12), $Y_{\rm L} = Z_{\rm L}^{-1}$ and $Y_{\rm S} = Z_{\rm S}^{-1}$ are the source and the load admittance satisfying the simultaneous conjugate matching condition as explained before. $I_{\rm S}$ is an arbitrary current source representing the excitation of the transmitting aperture. By combining (10), (11) and (12), the total electromagnetic field in the spectral domain is obtained. Then, we obtain the field distribution in the spatial domain by applying an inverse Hankel transform.

The time averaged Poynting vector $\boldsymbol{S}$ is thus derived as

$$\boldsymbol{S} = \frac{1}{2}\Re[\boldsymbol{E}_{\rm tot} \times \boldsymbol{H}^*_{\rm tot}], \tag{13}$$

in which $\boldsymbol{H}_{\rm tot}$ is the magnetic field in the spatial domain. The time averaged Poynting vector $\boldsymbol{S}$ is integrated over two infinite planes ($S_{\rm A}$ and $S_{\rm B}$) perpendicular to z-axis as shown in Fig. 1. $S_{\rm A}$ and $S_{\rm B}$ are very close (less than one tenth of the wavelength) to the transmitting and receiving aperture, respectively. The power leaving the transmitting aperture, or, equivalently, the power passing through $S_{\rm A}$ towards the receiving aperture, is derived as

$$P_{\rm in} = \iint_{S_{\rm A}} \boldsymbol{S} \cdot \hat{\boldsymbol{z}} dS. \tag{14}$$

Similarly, the power passing through $S_{\rm B}$ and flowing towards the receiving aperture, is derived as

$$P_{\rm out} = \iint_{S_{\rm B}} \boldsymbol{S} \cdot \hat{\boldsymbol{z}} dS. \tag{15}$$

It is worth observing that, since $S_{\rm A}(S_{\rm B})$ is very close to the transmitting (receiving) aperture, the normal component of the Poynting vector vanishes outside the area of the transmitting (receiving) aperture. Therefore, the derived power can be considered flowing exclusively through the radiating apertures.

The power transfer efficiency is then derived as

$$\eta = \frac{P_{\rm out}}{P_{\rm in}}. \tag{16}$$

C. T-factor approach

In [8], [13], [27], the power transfer efficiency or the transmission coefficient (T-factor) is derived by using the following expression

$$T = \frac{|\langle A, B\rangle|^2}{16 P_{\rm A} P_{\rm B}} \tag{17}$$

where $\langle A, B\rangle$ is the electromagnetic reaction between the transmitting and receiving apertures, yielding

$$\langle A, B\rangle = \iint_{S_{\rm A}} (\boldsymbol{E}_{\rm tot,B} \times \boldsymbol{H}_{\rm tot,A} + \boldsymbol{H}_{\rm tot,B} \times \boldsymbol{E}_{\rm tot,A}) \cdot \hat{\boldsymbol{z}} dS \tag{18}$$

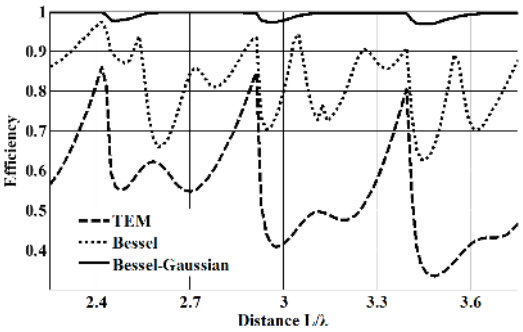

Fig. 3. Numerical results for the power transfer efficiency between apertures. The numerical results shown in the figure are obtained using the equivalent network approach. The dashed, dotted and solid curves correspond to TEM, BB, and BGB distributions, respectively.

with $\boldsymbol{E}(\boldsymbol{H})_{\rm tot,A}$ being the radiated electric (magnetic) when the transmitting aperture is excited; $\boldsymbol{E}(\boldsymbol{H})_{\rm tot,B}$ being the electric (magnetic) field when the receiving aperture is excited (for simplicity the radiated fields are derived over $S_{\rm A}$ in (18)); $P_{\rm A(B)}$ is the power radiated by the transmitting (receiving) aperture when the transmitting (receiving) aperture is excited. Since the two apertures under consideration are the same, we have

$$P_{\rm A(B)} = P_{\rm in} \tag{19}$$

As a result, combining (17), (18) and (19), the transmission coefficient is obtained.

D. Discussion

The equivalent network approach is the most computationally efficient and provides a network representation of the link which is useful for a practical implementation of the feeding system and for matching purposes. On the other hand, the equivalent network approach does not provide information on the electromagnetic field distribution between the radiating apertures which gives useful insight on the power transfer phenomenon. In particular, the power flow approach and the T-factor approach' approaches can be used to retrieve the field behavior between the transmitting and receiving apertures. The three approaches provide the same results, as we demonstrate in the following Section.

IV. Numerical Results and Analysis

In this section, numerical results of the power transfer efficiency between two radiating apertures are presented and discussed. In the following, TEM, BB, and BGB field distributions are considered.

For the TEM field distribution, the outer radius a and the inner radius b are arbitrarily chosen equal to 4λ and 0.4λ, respectively (refer to Fig. 1). For BB and BGB field distributions, we have chosen a circular aperture with a radius of 4λ and a $\rm TE_{01}$ BB distribution. The apodization width w_0 of the BGB is 3.38λ. Such value of the apodization factor corresponds to the minimum value of w_0 in which

This article has been accepted for publication in a future issue of this journal, but has not been fully edited. Content may change prior to final publication. Citation information: DOI 10.1109/OJAP.2021.3078234, IEEE Open Journal of Antennas and Propagation

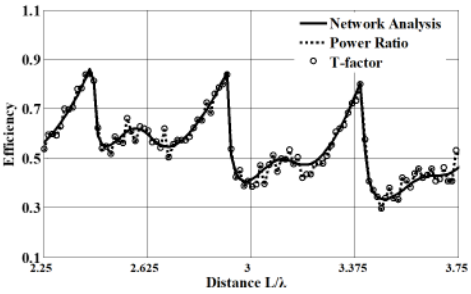

(a)

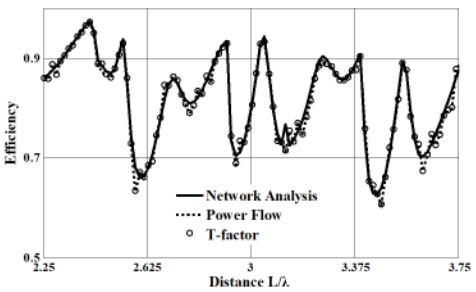

(b)

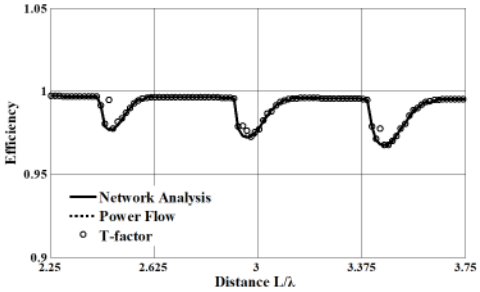

(c)

Fig. 4. Power transfer efficiency. The solid, dotted, and the circle lines are obtained using the equivalent network, the power flow, and T-factor approach, respectively. (a) TEM, (b) BB, and (c) BGB field.

$z_{\mathrm{ndr}}^{\mathrm{BB}} = z_{\mathrm{ndr}}^{\mathrm{BGB}}$. The non-diffractive range of both distributions is equal to 24λ and $k_1 \approx 0.15k_0$. The operating frequency f_0 is arbitrarily set to 2.5 GHz.

Fig. 3 shows the WPT performance of the analyzed beams in a short range of distances, namely from 2.25λ to 3.75. The power transfer efficiencies shown in Fig. 3 are derived using the equivalent network approach. In Fig. 4, we compare the WPT efficiency obtained using the three different methods described in the previous section. The results are in very good agreement validating the proposed approaches. According to Fig. 3, the BGB exhibits much higher power transfer efficiency than the TEM and slightly higher efficiency than the BB. Moreover, the BGB efficiency profile is much smoother compared to the two. This is attributed to the limited spectral content of its Fourier transform and lower diffraction around the edges of the aperture, as explained later. Several dips are evident in the efficiency figure (Fig. 3). As an example, let's consider the local minimum for the Bessel–Gauss distribution at $L \approx 2.94\lambda$. As previously stated, we approximate the radiating environment as a PPW formed by the infinite ground planes supporting the apertures at $z = 0$ and $L = 2.94\lambda$ (see Fig. 1). The Hankel transform of the equivalent magnetic current of the observed fields and spectral Green's function $G_{\phi\phi}^{\mathrm{HM}}$ of the PPW are shown in Fig. 5. The Hankel transform for the observed TEM, BB, and BGB peak at $k_\rho = 0.14k_0$, $k_\rho = 0.12k_0$ and at $k_\rho = 0.11k_0$, respectively, while the spectral Green's function exhibits a singularity at $k_\rho = 0.12k_0$. We can associate such singularity to a mode supported by the PPW environment excited by the equivalent magnetic current distributions over the apertures, and its position depends on the distance between the apertures (i.e., walls of the PPW). Since the peaks of the spectra of the observed beams overlap with the singularity of the Green's function, the mode is strongly excited. Therefore, the power is travelling outward between the ground planes and less power is captured by the receiving aperture. Such a phenomenon explains the dips in power transfer efficiency for the considered field distributions in Fig. 3. On the other hand, for distances corresponding to efficiency peaks, the singular point(s) of the relevant Green's function do not overlap with the spectrum of the magnetic current distributions of the observed fields. As a result, the resulting mode is marginally excited and, hence, more power is delivered to the receiving aperture.

Fig. 6 shows the electric field and the Poynting vector along the xz-plane, (refer to Fig. 1). Only the radial component of the electric field is reported since the azimuthal one is zero in the considered radiating environment. Besides, the z-component of the electric field does not contribute to the power flow towards the receiving aperture (z-direction). For similar reasons, only the z-component of the Poynting vector is reported. The non-diffractive nature of the BGB can be appreciated in Fig. 6(c), in contrast to Fig.6(a) for the coaxial TEM case. As for the BB, the electric field profile is distorted due to the diffraction around the edges of the aperture and a wider spectrum that can potentially excite higher-order modes of the radiating environment. Such distortion is much less present in the BGB, due to the radial tapering and a narrower spectrum. The difference between the considered

This article has been accepted for publication in a future issue of this journal, but has not been fully edited. Content may change prior to final publication. Citation information: DOI 10.1109/OJAP.2021.3078234, IEEE Open Journal of Antennas and Propagation

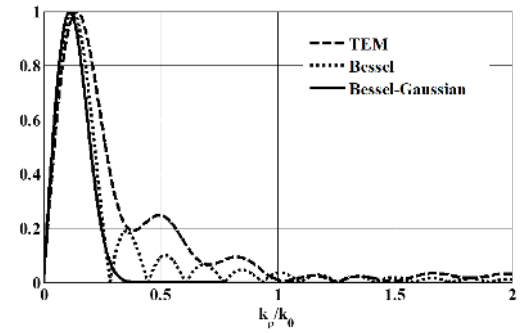

(a)

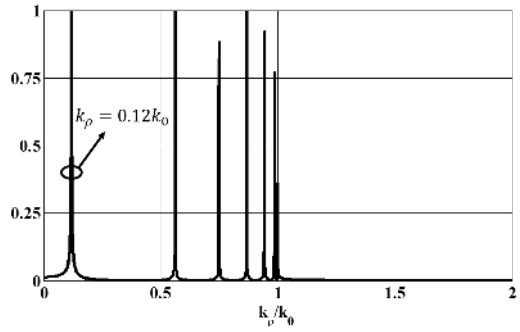

(b)

Fig. 5. (a) Normalized Hankel transform of TEM (dashed line), BB (dotted line), and BGB (solid line) field distributions. k_ρ/k_0 represents the spectral wavenumber normalized to the free space wavenumber. (b) Magnitude of the spectral Green's function component $G_{\phi\phi}^{\mathrm{HM}}$ of the equivalent PPW at $z = 0$ when $L = 2.94\lambda$.

field distributions is also evident from the Poynting vector, shown in the right side of Fig. 6. As shown in Fig.6(c), the distribution of the Poynting vector remains stable for the BGB along the z-direction and its transverse profile is very similar to the electric field distribution.

Finally, we will comment on the choice of the normalized apodization factor $\tilde{w}_0$. In our analysis, we have considered the border case of (5), i.e., $\tilde{w}_0 = 1/\sqrt{\ln 4}$. This value corresponds to the minimum value of $\tilde{w}_0$ in which the NDR of the BGB is equal to the NDR of the BB, i.e., the maximum width that does not reduce the non-diffractive range of the radiated beam. Clearly, there is no benefit of using broader apodization windows since we would only introduce stronger edge components that can lead to more diffraction without increasing the range of our WPT system. On the other hand, narrower apodizations, despite reducing the NDR, can further reduce the diffraction effects.

V. Bessel–Gauss Beam Launchers for WPT

A. Synthesized Launcher

We have demonstrated recently that circular metallic horns can be shaped in such a way to allow radiation of Bessel beams in a wide range of frequencies [22]. We have implemented an ad-hoc tool based on mode matching [32] to synthesize horns that convert a circular TE_{01} mode field distribution at the input waveguide to a Bessel distribution at the radiating aperture. We assume that we can generate the circular TE_{01}

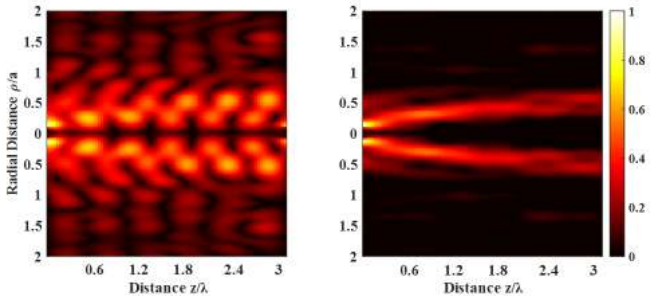

(a) coaxial TEM

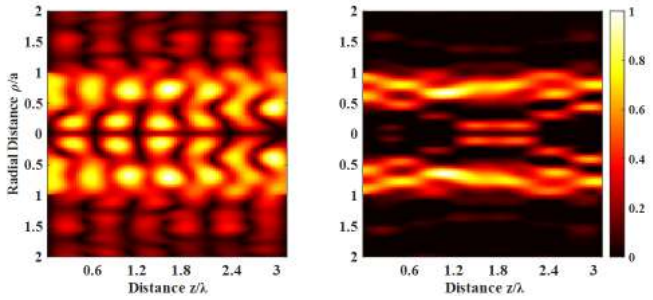

(b) Bessel

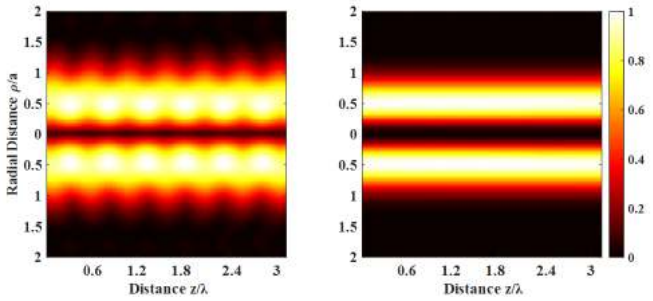

(c) Bessel–Gauss

Fig. 6. Normalized amplitudes of the E-field and the z-component of the Poynting vector in the $x0z$ plane between two apertures when $L = 3.15\lambda$. The electric field is plotted on the left, and the Poynting vector is plotted on the right. (a) TEM, (b) BB, and (c) BGB distribution.

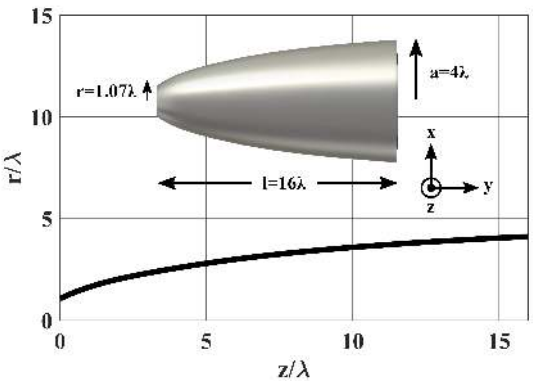

Fig. 7. Dimensions of the realized BGB launcher normalized to the wavelength. Inset: Synthesized metal horn.

This article has been accepted for publication in a future issue of this journal, but has not been fully edited. Content may change prior to final publication. Citation information: DOI 10.1109/OJAP.2021.3078234, IEEE Open Journal of Antennas and Propagation

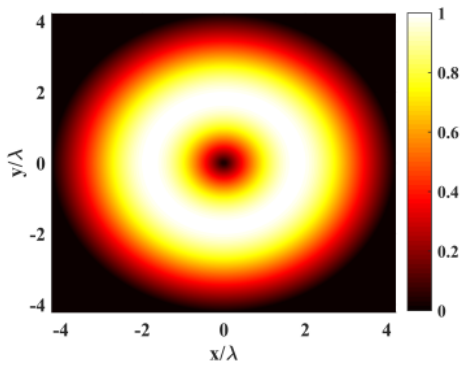

Fig. 8. Normalized amplitude of the BGB electric field distribution at the aperture of the launcher.

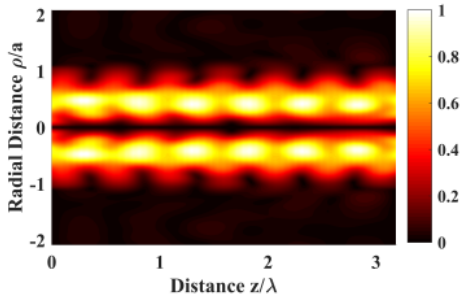

Fig. 9. Normalized simulated amplitudes of the E-field of the BGB launcher in the $x0z$ plane between two apertures when $L = 3.15\lambda$.

field distribution using well-known mode converters, e.g. [33], [34].

Applying a similar procedure, we have synthesized a circular metallic horn that converts a TE_{01} mode at the input to a Bessel–Gauss field distribution at the aperture. The BGB distribution is synthesized by optimizing the far-field distribution of the horn to match the far-field distribution of the target distribution, which is a TE_{01} mode with a prescribed radius a windowed by a Gaussian function with a prescribed apodization factor w_0. In our case, the operating frequency of the launcher is 2.5 GHz and its aperture radius, apodization factor, and non-diffractive range correspond to those mentioned in the previous section, i.e. 4λ, 3.38λ, and $24\lambda_0$. Fig. 7 shows the synthesized launcher. The curved profile is a cubical spline defined by its control points shown in Table I. Finally, Fig. 8 shows the E-field distribution at the aperture.

Next, we simulated a WPT link that consists of two BGB launchers from the previous subsection, with their apertures aligned as sketched in Fig. 1. The distance between the two launchers was arbitrarily set to $L = 3.15\lambda$. The simulation was performed using time domain solver of CST Microwave Studio

TABLE I
CONTROL POINTS OF THE SPLINE PROFILE DEFINING THE BGB LAUNCHER

l/λ	0	2.64	2.81	11	15.76	15.83	16.04
r/λ	1.04	2.21	2.26	3.69	4	4.02	4.03

[35] and the obtained power transfer efficiency is close to 100%, corresponding to the value we obtained in the previous section for the same distance between the two apertures. Fig. 9 shows the simulated amplitude of the electric field of the WPT link along the $x0z$ plane and the good agreement with 6(c) validates the calculation method.

B. Frequency Tuning

In Section IV, the maxima and minima of the power transfer efficiency have been explained by studying the spectra of the equivalent magnetic currents and the relevant component of the dyadic Green's function of the PPW environment. We have concluded that the efficiency depends on the excitation of the propagating modes supported by the PPW environment formed by the two ground planes of the radiating apertures. Fig. 3 and Fig. 10 show the efficiency of the BGB field for distances ranging from 2.25λ to 30λ. When the distance between the two radiating apertures is small ($L \approx 3\lambda$), the amplitude oscillations in power transfer efficiency are less than 5%. However, when the distance increases, the efficiency fluctuations become more evident and the oscillations exceed 30% at $L \approx 21\lambda$. One possible way to stabilize the efficiency performance is to tune the operating frequency of the WPT systems at each separation distance. This is an approach typically used for resonant-inductive links [36].

The frequency tuning technique is based on knowledge of the equivalent current spectrum distribution and the spectral Green's function of the radiating environment for the structures under consideration. The idea is to tune the operating frequency to avoid the excitation of a guided mode of the radiating environment. An example is provided next for the BGB launcher from the previous section.

As shown in Fig. 10, the WPT efficiency versus distance exhibits an oscillating behavior if no frequency tuning is employed. However, we can suppress the oscillatory behavior by employing a frequency tuning technique. Consider the local minimum in efficiency at $L \approx 14.7\lambda$. The spectrum of the equivalent current distribution and of the spectral Green's function are shown in Fig. 11. It is clear from Fig. 11 that two PPW modes are excited. The radial wavenumber k_ρ associated with the modes is given by [23]

$$\frac{k_\rho}{k_0} = \sqrt{1 - \left(\frac{n\pi}{Lk_0}\right)^2} \tag{20}$$

where

$$n = \left\lfloor \frac{Lk_0}{\pi} \right\rfloor, \left\lfloor \frac{Lk_0}{\pi} \right\rfloor - 1 \tag{21}$$

In (20) and (21), n is the order of a PPW mode. In this context, the mode with the higher order ($n = 30$, the first singularity in Fig. 11) is the dominant one and is strongly excited. This results in a sharp drop in efficiency in the neighborhood of $L = 14.7\lambda$. According to (20), the ratio of k_ρ/k_0 becomes larger if k_0 (operating wavenumber) increases. In other words, the pole in Fig. 11 moves toward larger normalized transverse

This article has been accepted for publication in a future issue of this journal, but has not been fully edited. Content may change prior to final publication. Citation information: DOI 10.1109/OJAP.2021.3078234, IEEE Open Journal of Antennas and Propagation

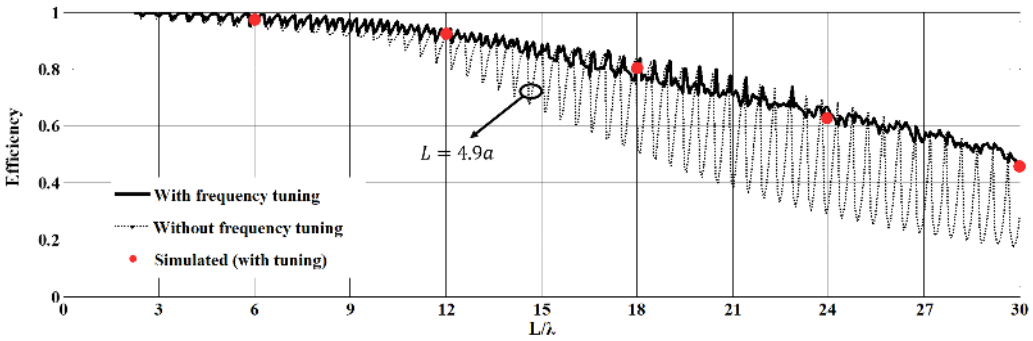

Fig. 10. Numerical results with (solid lines) and without (dashed lines) frequency tuning, and simulated results with frequency tuning for the power transfer efficiency between two BGB apertures

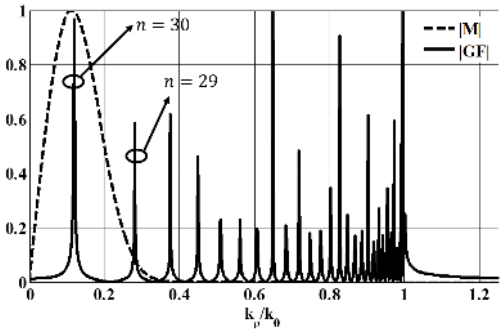

Fig. 11. Comparison of the normalized Hankel transform of the BGB field distribution (dashed line) and the magnitude of the spectral Green's function component $G_{\phi\phi}^{\mathrm{HM}}$ (solid line) at $z = 0$, $L = 14.7\lambda$, $f_0 = 2.5$ GHz. k_ρ/k_0 represents the spectral wavenumber normalized to the wavenumber in free space.

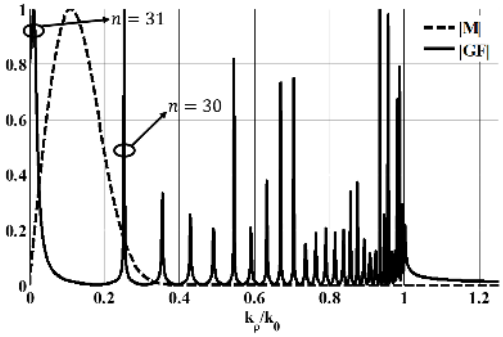

Fig. 12. Comparison of the normalized Hankel transform of the BGB field distribution (dashed line) and the magnitude of the spectral Green's function component $G_{\phi\phi}^{\mathrm{HM}}$ (solid line) at $z = 0$, $L = 14.7\lambda$, $f_0 = 2.565$ GHz. k_ρ/k_0 represents the spectral wavenumber normalized to the wavenumber in free space.

wavenumber values and the excitation of the mode of order 30 is avoided as k_0 increases. At the same time, an increase in frequency could potentially lead to the excitation of the next, higher-order mode (of order 31, the first singularity in Fig. 12). The k_0' at which the next mode is excited can be obtained as

$$\left\lfloor \frac{Lk_0}{\pi} \right\rfloor + 1 = \frac{Lk_0'}{\pi} \tag{22}$$

Therefore, by properly tuning the k_0, the excitation of the PPW mode of order 30 and 31 can be avoided, as shown in Fig. 12. As a result the WPT efficiency is increased to 88% from 70% by tuning the operating frequency from 2.5 GHz to 2.565 GHz.

The tuning procedure explained above can be applied at each operating distance. Fig. 10 shows the WPT efficiency under frequency tuning for the two radiating apertures of the previous section. We also show simulated results for the efficiency between the two launchers at distances of 6, 12, 18, 24, and 30λ under frequency tuning. The tuning band is set to $2.5 - 2.57$ GHz. These results show that frequency tuning is a valid option to stabilize the efficiency over distances larger than 30λ. The efficiency of the BGB launcher proves to be higher than 60% within its non-diffractive range. Finally, it is worth mentioning that, other than the trade-off between the size of the launcher and the achieved non-diffractive range, the design procedure has no particular limitations in terms of non-diffractive range, as stated in Section V of [22]. Hence, the procedure can synthesize BGB launchers capable of transferring power wirelessly over arbitrarily long distances with high efficiency.

VI. Conclusions

In this paper, we proposed the use of Bessel–Gauss launchers for WPT. Three approaches for characterizing power transfer efficiency between two aligned radiating apertures are presented. In one case, the equivalent network representation of the coupled system is derived to evaluate power efficiency under a simultaneous conjugate impedance match. In the other two approaches, the efficiency is derived by resorting to the total electromagnetic field radiated by the apertures. The proposed methods are used to evaluate power transfer efficiency for two apertures facing each other, with field profiles equal to a coaxial TEM, BB, and BGB aperture fields. We have demonstrated that the BGB field exhibits higher performance in terms of power transfer efficiency. The higher efficiency is attributed to the non-diffractive nature of the generated fields,

reduced diffraction around the edges, and its limited spectrum. We synthesized a BGB launcher with power transfer efficiency exceeding 50% for distances larger than 30 wavelengths, i.e., even beyond the NDR of the generated beam. Calculated results are in good agreement with full-wave simulations. A fluctuating efficiency is observed for long distances of operation. Such fluctuations are due to the excitation of guided modes between the two radiating apertures. Frequency tuning is thus proposed to stabilize the efficiency (reduce fluctuations) for large distances. The proposed system will enhance the power transfer efficiency and operating range of current WPT systems.

REFERENCES

[1] N. Tesla, "System of transmission of electrical energy," United States Patent 645576, Mar. 1900.

[2] A. Kurs, A. Karalis, R. Moffatt, J. D. Joannopoulos, P. Fisher, and M. Soljačić, "Wireless Power Transfer via Strongly Coupled Magnetic Resonances," *Science*, vol. 317, no. 5834, pp. 83-86, Jul. 2007.

[3] S. Y. R. Hui, W. Zhong, and C. K. Lee, "A Critical Review of Recent Progress in Mid-Range Wireless Power Transfer," *IEEE Trans. Power Electron.*, vol. 29, no. 9, pp. 4500-4511, Mar. 2013.

[4] J. Garnica, R. A. Chinga, and J. Lin, "Wireless Power Transmission: From Far Field to Near Field," in *Proc. IEEE*, vol. 101, no. 6, pp. 1321-1331, Jun. 2013.

[5] B. Strassner and K. Chang "Microwave Power Transmission: Historical Milestones and System Components," in *Proc. IEEE*, vol. 101, no. 6, pp. 1379-1396, Mar. 2013.

[6] "Wireless Power Consortium," http://www.wirelesspowerconsortium.com.

[7] "Airfuel Alliance," http://www.airfuel.org/about-airfuel.

[8] G. Borgiotti, "Maximum power transfer between two planar apertures in the Fresnel zone," *IEEE Trans. Antennas Propag.*, vol. 14, no. 2, pp. 158-163, Mar. 1966.

[9] J. Heebl, M. Ettorre, and A. Grbic, "Wireless links in the radiative near field via Bessel beams," *Phys. Rev. Applied*, vol. 6, no. 3, p. 034018, Sep. 2016.

[10] J. Durnin, "Exact solutions for nondiffracting beams. I. The scalar theory," *J. Opt. Soc. Am. A,* , vol. 4, no. 4, pp. 651-654, Apr. 1987.

[11] Y. Urzhumov and D. R. Smith, "Metamaterial-enhanced coupling between magnetic dipoles for efficient wireless power transfer," *Phys. Rev. B*, vol. 83, no. 20, p. 205114, May 2011.

[12] S. Kim, J. S. Ho, and S. Y. Poon, "Midfield Wireless Powering of Subwavelength Autonomous Devices," *Phys. Rev. Lett.*, vol. 110, no. 20, p. 203905, May 2013.

[13] F. Alsolamy, W. Alomar, and A. Grbic, "Cylindrical Vector Beams for Wireless Power Transfer," *IEEE Trans. Antennas Propag.*, vol.69, no. 3, pp. 1716-1727, Mar. 2021.

[14] F. Gori, G. Guattari, and C. Padovani, "Bessel–Gauss beam," *Opt. Commun.*, vol. 64, no. 6, pp. 491-495, Dec. 1987.

[15] V. Bagini, F. Frezza, M. Santarsiero, G. Schettini, and G. S. Spagnolo, "Generalized Bessel–Gauss beams," *J. Mod. Opt.*, vol. 43, no. 6, pp. 1155-1166, 1996.

[16] S. Chávez-cerda, "A new approach to bessel beams," *J. Mod. Opt.*, vol. 46, no. 6, pp. 923-930, 1999.

[17] W. Fuscaldo, A. Benedetti, D. Comite, P. Baccarelli, P. Burghignoli, and A. Galli, "Bessel–Gauss Beams Through Leaky Waves: Focusing and Diffractive Properties," *Phys. Rev. Applied*, vol. 13, no. 6, p. 064040, Jun. 2020.

[18] M. Anguiano-Morales, A. Martinez, M. David Iturbe-Castillo, S. Chávez-Cerda, and N. Alcála-Ochoa, "Self-healing property of a caustic optical beam," *Appl. Opt.*, vol. 46, no. 34, pp. 8284-8290, Nov. 2007.

[19] P. L. Overfelt and C. S. Kenney, "Comparison of the propagation characteristics of Bessel, Bessel-Gauss, and Gaussian beams diffracted by a circular aperture," *J. Opt. Soc. Am. A,* vol. 8, no. 5, pp. 732-745, May 1991.

[20] J. Mendoza-Hernández, M. L. Arroyo-Carrasco, M. D. Iturbe Castillo, and S. Chávez-Cerda, "Laguerre-Gauss beams versus Bessel beams showdown: peer comparison," *Opt. Lett.*, vol. 40, no. 16, pp. 3739-3742, Aug. 2015.

[21] W. Fuscaldo, P. Burghignoli, and A. Galli, "A comparative analysis of Bessel and Gaussian beams beyond the paraxial approximation," *Optik*, vol. 240, p. 166834, Mar. 2021.

[22] S. Paković, N. Bartolomei, M. J. Mencagli, M. Ettorre, R. Sauleau, and D.González-Ovejero, "A Fast and Accurate Method of Synthesizing X-Wave Launchers by Metallic Horns," *IEEE Access*, vol. 9, pp. 1996-2006, Dec. 2020.

[23] D. M. Pozar, *Microwave Engineering, 4th edition*. New York: Wiley, 2011.

[24] M. Ettorre, S. C. Pavone, M. Casaletti, M. Albani, A. Mazzinghi, and A. Freni, "Near-field focusing by non-diffracting Bessel beams," in *Aperture Antennas for Millimeter and Sub-Millimeter Wave Applications*, A. Boriskin and R. Sauleau, Eds., Springer, 2017.

[25] M. Ettorre and A. Grbic, "Generation of Propagating Bessel Beams Using Leaky-Wave Modes," *IEEE Trans. Antennas Propag.*, vol. 60, no. 8, pp. 3605-3613, Aug. 2012.

[26] M. Ettorre and A. Grbic, "Generation of Propagating Bessel Beams Using Leaky-Wave Modes: Experimental Validation," *IEEE Trans. Antennas Propag.*, vol. 60, no. 6, pp. 2645-2653, Jun. 2012.

[27] M. K. Hu, "Near-zone power transmission formulas," *IRE Natl. Conv. Rec.*, vol. 6, pp. 128-135, 1958.

[28] A. Neto, N. Llombart, G. Gerini, M. Bonnedal, and P. J. I. de Maagt, "EBG enhanced feeds for the improvement of the aperture efficiency of reflector antennas," *IEEE Trans. Antennas Propag.*, vol. 55, no. 8, pp. 2185-2193, Aug. 2007.

[29] N. Llombart, A. Neto, G. Gerini, M. Bonnedal, and P. J. I. de Maagt, "Impact of mutual coupling in leaky wave imaging arrays," *IEEE Trans. Antennas Propag.*, vol. 56, no. 4, pp. 1201-1206, Apr. 2008.

[30] R. F. Harrington, *Time-harmonic electromagnetic fields*, New York: Wiley, 2001.

[31] M. Ettorre and A. Grbic, "A transponder-based, non-radiative wireless power transfer," *IEEE Antennas Wirel. Propag. Lett.*, vol. 11, pp. 1150-1153, Sep. 2012.

[32] G. Conciauro, M. Gugilelmi, and R. Sorrentino, *Advanced Modal Analysis*. New York: Wiley, 2000.

[33] S. S. Saad, J. B. Davies, and O. J. Davies, "Analysis and design of a circular TE01 mode transducer," *IEE J. Microwave Opt. Acoust.*, vol. 1, no. 2, pp. 58-62, Jan. 1977.

[34] C.-F. Yu and T.-H. Chang, "High-performance circular TE_{01}-mode converter," *IEEE Trans. Microw. Theory Tech.*, vol. 53, no. 12, pp. 3794-3798, Dec. 2005.

[35] CST Microwave Studio, CST Amer., Anaheim, CA, USA, 2016.

[36] J. D. Heebl, E. M. Thomas, R. P. Penno, and A. Grbic, "Comprehensive analysis and measurement of frequency-tuned and impedance-tuned wireless non-radiative power-transfer systems," *IEEE Antennas Propag. Mag.*, vol. 56, no. 5, pp. 131-148, Oct. 2014.

Srđan Paković received the B.S. and M.S. degrees in electrical engineering from the Univerzitet u Beogradu, Elektrotehnički fakultet, Belgrade, Serbia, in 2017. In 2018, he joined Institut d'Électronique et des Technologies du numéRique (IETR), Rennes, France, where he is currently pursuing a Ph.D. degree in electronics. His research interests include non-diffractive waves, near-field focusing, wireless power transfer, and computational electromagnetics.

This article has been accepted for publication in a future issue of this journal, but has not been fully edited. Content may change prior to final publication. Citation information: DOI 10.1109/OJAP.2021.3078234, IEEE Open Journal of Antennas and Propagation

David González-Ovejero (S'01–M'13–SM'17) was born in Gandía, Spain, in 1982. He received the M.S. degree in telecommunication engineering from the Universidad Politécnica de Valencia, Valencia, Spain, in 2005, and the Ph.D. degree in electrical engineering from the Université catholique de Louvain, Louvain-la-Neuve, Belgium, in 2012. From 2012 to 2014, he was a Research Associate with the University of Siena, Siena, Italy. In 2014, he joined the Jet Propulsion Laboratory, California Institute of Technology, Pasadena, CA, USA, where he was a Marie Curie Post-Doctoral Fellow. Since 2016, he has been a tenured researcher with the French National Center for Scientific Research (CNRS), Institut d'Electronique et des Technologies du numéRique (IETR), Rennes, France. His current research interests include computational electromagnetics, large phased arrays, periodic structures, metasurfaces and submillimeter wave antennas. Dr. González-Ovejero was a recipient of a Marie Curie International Outgoing Fellowship from the European Commission 2013, the Sergei A. Schelkunoff Transactions Prize Paper Award from the IEEE Antennas and Propagation Society in 2016, the Best Paper Award in Antenna Design and Applications at the 11th European Conference on Antennas and Propagation in 2017, and the Best Paper Award in Electromagnetics at the 15th European Conference on Antennas and Propagation in 2021. Since 2019, he has been an Associate Editor of the IEEE TRANSACTIONS ON ANTENNAS AND PROPAGATION and the IEEE TRANSACTIONS ON TERAHERTZ SCIENCE AND TECHNOLOGY.

Santi C. Pavone (S'13 – M'16 – SM'20) received the B.Sc. and M.Sc. degrees (both summa cum laude) in electronics engineering from the University of Messina, Messina, Italy, in 2010 and 2012, respectively, and the Ph.D. degree (with the additional label of "Doctor Europaeus") in information engineering and science (electromagnetics engineering) from the University of Siena, Siena, Italy, in 2015. He was visiting Ph.D. student and Assistant Professor at the Institut d'Électronique et de Télécommunications de Rennes (IETR), Université de Rennes 1, Rennes, France, in 2015 and 2020, respectively. From 2016 to July, 2019, he was an Associate Researcher with the Laboratory of Applied Electromagnetics, University of Siena, Siena, Italy. Since August, 2019, he is an Assistant Professor at the Department of Electrical, Electronics, and Information Engineering (DIEEI), University of Catania, Italy. His current research interests include fundamental electromagnetic theory, scattering theory, RADAR design at millimeter waves, high-frequency techniques, focusing systems, non-diffractive localized pulses, and reconfigurable antennas. Dr. Pavone was a recipient of the ESF Research Networking Programme NEW-FOCUS Scholarship in 2015, and also of the IEEE Antennas and Propagation Society Student Award, Chapter Central-Southern Italy, in 2014. In 2017, he was a finalist for the Best Paper Award in Electromagnetics and Antenna Theory at the 11th European Conference on Antennas and Propagation, Paris. In 2018 he was co-recipient of the Best Paper Award in Electromagnetics and Antenna Theory at the 12th European Conference on Antennas and Propagation, London, UK. In 2019, he was the recipient of the Young Scientist Award (YSA) at the 41st Progress in Electromagnetics Research Symposium (PIERS 2019), held in Rome, Italy. In 2020, he got the National Scientific Habilitation for Associate Professorship of Electromagnetic Fields by the Italian Ministry of University and Research (MUR), and he has been selected among the outstanding 100 reviewers for the IEEE Transactions on Antennas and Propagation (reference period: June 2019 – May, 2020). He serves as an Associate Editor for IEEE Access and IET Electronics Letters.

Anthony Grbic (S'00 - M'06 - SM'14 – F'16) received the B.A.Sc., M.A.Sc., and Ph.D. degrees in electrical engineering from the University of Toronto, Canada, in 1998, 2000, and 2005, respectively. In 2006, he joined the Department of Electrical Engineering and Computer Science, University of Michigan, Ann Arbor, MI, USA, where he is currently a Professor. His research interests include engineered electromagnetic structures (metamaterials, metasurfaces, electromagnetic band-gap materials, frequency-selective surfaces), antennas, microwave circuits, plasmonics, wireless power transmission, and analytical electromagnetics/optics.

Dr. Grbic served as Technical Program Co-Chair in 2012 and Topic Co-Chair in 2016 and 2017 for the IEEE International Symposium on Antennas and Propagation and USNC-URSI National Radio Science Meeting. He was an Associate Editor for IEEE Antennas and Wireless Propagation Letters from 2010 to 2015. Dr. Grbic was the recipient of AFOSR Young Investigator Award as well as NSF Faculty Early Career Development Award in 2008, the Presidential Early Career Award for Scientists and Engineers in January 2010. He also received an Outstanding Young Engineer Award from the IEEE Microwave Theory and Techniques Society, a Henry Russel Award from the University of Michigan, and a Booker Fellowship from the United States National Committee of the International Union of Radio Science in 2011. He was the inaugural recipient of the Ernest and Bettine Kuh Distinguished Faculty Scholar Award in the Department of Electrical and Computer Science, University of Michigan in 2012. In 2018, Prof. Anthony Grbic received a University of Michigan Faculty Recognition Award for outstanding achievement in scholarly research, excellence as a teacher, advisor and mentor, and distinguished service to the institution and profession.

Mauro Ettorre (Senior Member, IEEE) received a Laurea degree "summa cum laude" in Electrical Engineering, and a Ph.D. degree in Electromagnetics from the University of Siena, Italy, in 2004 and 2008, respectively. Part of his Ph.D. work was developed at the Netherlands Organisation for Applied Scientific Research (TNO), The Hague, the Netherlands, where he later worked as an Antenna Researcher. From 2008 to 2010, Dr. Ettorre was a Postdoctoral Fellow at Institut d'Electronique et de Télécommunications de Rennes (IETR), University of Rennes 1, France. In 2010 and 2016, he was a Visiting Scholar in the Radiation Laboratory, Department of Electrical Engineering and Computer Science, University of Michigan, USA. Since October 2010, he is a Research Scientist at the Centre National de la Recherche Scientifique (CNRS), within the IETR. In 2014, he assumed responsibilities for the multi-beam antenna activity for satellite applications in the joint laboratory between IETR and Thales Alenia Space, France. In 2015, he was an Invited Professor at the Tokyo Institute of Technology (TIT), Japan. Since 2016, he has been Secretary of the French National Committee for Scientific Research, Section 08 (micro- and nanotechnologies, photonics, electromagnetism), CNRS, Paris, France. Since 2017, he is an Associate Editor for the IEEE Transaction on Antennas and Propagation. In 2017, 2018, and 2019 he was a member of the best paper award selection committee for the IEEE Transactions on Terahertz Science and Technology.

Dr. Ettorre's research interests include the analysis and design of leaky-wave antennas, periodic structures, millimeter-wave antennas, non-diffractive radiation and localized waves, near-field focusing techniques, and wireless power transfer systems.

Dr. Ettorre received the Young Antenna Engineer Prize at the 2008 ESA Antenna Workshop in the Netherlands, the Innovation Award at 2018 ESA Antenna Workshop in the Netherlands and the Best Paper Award in Electromagnetics and Antenna Theory at the 2018 European Conference on Antennas and Propagation (EuCAP), London, UK.